Cell Tissue Res. 279, 13 (1995).
13. The vesicle extract was run through a Bio-Rad Econo-Pac 10DG (Bio-Gel P-6DG) column, which has an exclusion limit of 6000 daltons and a fractionation range of 1000 to 6000 daltons.
14. J. B. Fenn et al., Science 246, 64 (1989).
15. The entire vesicle extract was electrosprayed into a Fourier-transform mass spectrometer. The two most abundant peaks were at m/z 144 and 118; ions corresponding to NTPs were observed in minor abundance.
16. Low-resolution ESI mass spectra were acquired on a home-built electrospray ionization quadrupole mass spectrometer, which is described in more detail in S. E. Rodriguez-Cruz, J. S. Klassen, E. R. Williams, J. Am. Soc. Mass Spectrom. 8, 565 (1997).
17. E. R. Williams, Trends Anal. Chem. 13, 247 (1994); D. S. Gross and E. R. Williams, J. Am. Chem. Soc. 117, 883 (1995).
18. Exact masses were determined from four replicate measurements with a mass accuracy of better than 10 parts per million using internal calibration standards. Elemental compositions were assigned on the basis of the masses of the common elements and were constrained by the measured isotope distributions.
19. High-performance LC was run with a 25-cm-long column using two different mobile phase compositions (phosphate buffer at pH 5.40 and 6.50), with methanol as the organic modifier. Derivatization with o-phthalaldehyde/β-mercaptoethanol and reversed-phase LC was performed according to P. Lindroth and K. Mopper, Anal. Chem. 51, 1667 (1979), with minor modifications [X. Li, A. Hallqvist, I. Jacobson, O. Orwar, M. Sandberg, Brain Res. 706, 86 (1996)]. Detection was performed with the use of a deuterium light source (excitation: 330 nm; detection: 418 nm). Standard addition of taurine to the samples yielded high recoveries: 105% (pH = 5.40, n = 3) and 104% (pH = 6.50, n = 3).
20. R. McCaman and J. Stetzler, J. Neurochem. 29, 739 (1977).
21. R. J. Huxtable, Physiol. Rev. 72, 101 (1992).
22. We thank P. Schnier, R. Jockusch, and J. Klassen for technical assistance with mass spectrometry. We also thank G. T. Nagle and S. D. Painter for generously providing us with purified atrial gland peptides. S.J.L. acknowledges support from NIH for a postdoctoral fellowship (GM18386). O.O. is supported by the Swedish Natural Science Research Council (NFR) (10481-305, -308, and -309) and by the Swedish Foundation for Strategic Research (SSF). M.S. is supported by NFR (01-905-313). This work is supported by the International Joint Research Program (NEDO) of Japan, the U.S. National Institute on Drug Abuse (DA09873), NSF (CHE-9258178), and NIH (1R29GM50336-01A2).

17 September 1997; accepted 13 January 1998

Images of Interlayer Josephson Vortices in $Tl_2Ba_2CuO_{6+\delta}$

Kathryn A. Moler,* John R. Kirtley, D. G. Hinks, T. W. Li, Ming Xu†

The strength of the interlayer Josephson tunneling in layered superconductors is an essential test of the interlayer tunneling model as a mechanism for superconductivity, as well as a useful phenomenological parameter. A scanning superconducting quantum interference device (SQUID) microscope was used to image interlayer Josephson vortices in $Tl_2Ba_2CuO_{6+\delta}$ and to obtain a direct measure of the interlayer tunneling in a high–transition temperature superconductor with a single copper oxide plane per unit cell. The measured interlayer penetration depth, λ_c, is ~20 micrometers, about 20 times the penetration depth required by the interlayer tunneling model.

Although tremendous progress has been made over the past decade in understanding the phenomenological properties of the cuprate superconductors, in improving the quality of the materials, and in identifying the symmetry of the pairing state, the mechanism of the superconductivity remains unresolved. One candidate mechanism is the interlayer tunneling (ILT) model, in which the superconductivity results from an increased coupling between the layers in the superconducting state (1–3). For this model to succeed, the interlayer coupling in the superconducting state must be sufficiently strong to account for the large condensation energy of the cuprate superconductors (3–5). The best materials for testing this requirement are $Tl_2Ba_2CuO_{6+\delta}$ (Tl-2201) and $HgBa_2CuO_{4+\delta}$ (Hg-1201), which have high critical temperatures ($T_c \approx 90$ K) and a single copper oxide plane per unit cell.

K. A. Moler, Department of Physics, Princeton University, Princeton, NJ 08544, USA.
J. R. Kirtley, IBM T. J. Watson Research Center, Post Office Box 218, Yorktown Heights, NY 10598, USA.
D. G. Hinks and T. W. Li, Materials Science Division, Argonne National Laboratory, Argonne, IL 60439, USA.
M. Xu, James Franck Institute, University of Chicago, Chicago, IL 60637, USA.

*To whom correspondence should be addressed.
†Present address: Lucent Technologies, 2000 North Naperville Road, Naperville, IL 60566, USA.

The interlayer tunneling strength in cuprates is often inferred from the normal-state anisotropy, but a key point of the ILT model is that this correlation will be unconventional in the single-layer cuprates. It is therefore crucial to determine the interlayer coupling in the superconducting state. One measure of this coupling is the c-axis magnetic penetration depth, λ_c. Another measure is the Josephson plasma frequency (6, 7), $\omega_p = c\lambda_c^{-1}\varepsilon^{-1/2}$, where ε is the dielectric constant of the interlayer medium and c is the speed of light. The Josephson resonance has not been detected in either Tl-2201 or Hg-1201. Van der Marel and colleagues reported an upper limit $\omega_p \varepsilon^{1/2} < 100$ cm^{-1} in Tl-2201 (8), a value difficult to explain within the ILT model (4). In contrast, recently measured magnetic susceptibility data on oriented powders of Hg-1201, analyzed with London's equation and assuming spherical grains, give $\lambda_c(T = 0) = 1.36 \pm 0.16$ μm for Hg-1201 (9), similar to the ILT value (10). Here, we used a SQUID microscope to image interlayer Josephson vortices in two single crystals of Tl-2201 and determine λ_c directly.

The phenomenological Lawrence-Doniach model for a stack of Josephson-coupled superconducting layers (6) is widely applied to highly anisotropic superconductors, including organics, cuprates, and artificially structured model systems. The structure of an isolated vortex parallel to the layers, or "interlayer Josephson vortex," is similar to a vortex in an anisotropic Ginzburg-Landau theory except at the vortex core (11). The spatial extent of the vortex along the layers, λ_c, is related to the critical current density between the layers, J_0, by

$$\lambda_c = (c\Phi_0/8\pi^2 s J_0)^{1/2} \quad (1)$$

(6, 11), where $\Phi_0 = hc/2e$ is the superconducting flux quantum, h is Planck's constant, e is the electron charge, and s is the interlayer spacing. A large vortex thus indicates a weak interlayer coupling.

In recent work, we used vortex imaging to directly measure the Josephson coupling across grain boundaries of $YBa_2Cu_3O_{7-\delta}$ (12) and the interlayer Josephson coupling in the quasi-two-dimensional (quasi-2D) organic superconductor κ-(BEDT-TTF)$_2$-Cu(NCS)$_2$ (13). We now report the observation of isolated interlayer vortices in $Tl_2Ba_2CuO_{6+\delta}$. Although the a-axis penetration depth is substantially less than our spatial resolution of 8 μm, our images directly show the c-axis penetration depth $\lambda_c \approx 20$ μm.

Magnetic fields were imaged at the surface of the crystals with a scanning SQUID microscope (14). The SQUID is integrated with shielded leads to a square superconducting pickup loop (side length $L = 8.2$ μm) on the same chip. The SQUID detects the total magnetic flux through the pickup loop,

$$\Phi_s = \int_{\text{loop}} B_z(x, y, z = z_0)\,dx\,dy \quad (2)$$

where B_z is the local magnetic field perpendicular to the sample surface, x and y are parallel to the surface, and the distance z_0 between the surface and the pickup loop is typically a few micrometers. Although z_0 is known approximately from the experimental setup, in practice the exact value of z_0 at low temperatures should be considered an unknown. We detect the change in the flux through the pickup loop while scanning the sample in x and y, so that the signal for each data set has an arbitrary constant offset. When the 8.2-μm pickup loop is used to image an anisotropic vortex in Tl-2201 (Fig. 1A), the interlayer spacing, s = 11.6 Å, and the a-axis penetration depth, λ_a = 0.17 μm (*15*), are both smaller than the spatial resolution. The interlayer penetration depth λ_c corresponds to currents flowing between the layers (along the c axis).

We have previously imaged vortices in niobium films (*14*) and *ab*-plane vortices in $YBa_2Cu_3O_{7-\delta}$ (YBCO) films (*12*) and crystals (*16*). In these cases, the relevant penetration depths are much smaller than the size of the pickup loop, so the vortices are well approximated by monopole sources of magnetic flux (*17, 18*). Figure 1B shows images of two *ab*-plane vortices in YBCO, whose apparent shapes are determined by the shape of the pickup loop (*19*). In contrast, the interlayer vortices observed in images of the *ac* face of Tl-2201 (Fig. 1C) extend a considerable distance along the layers.

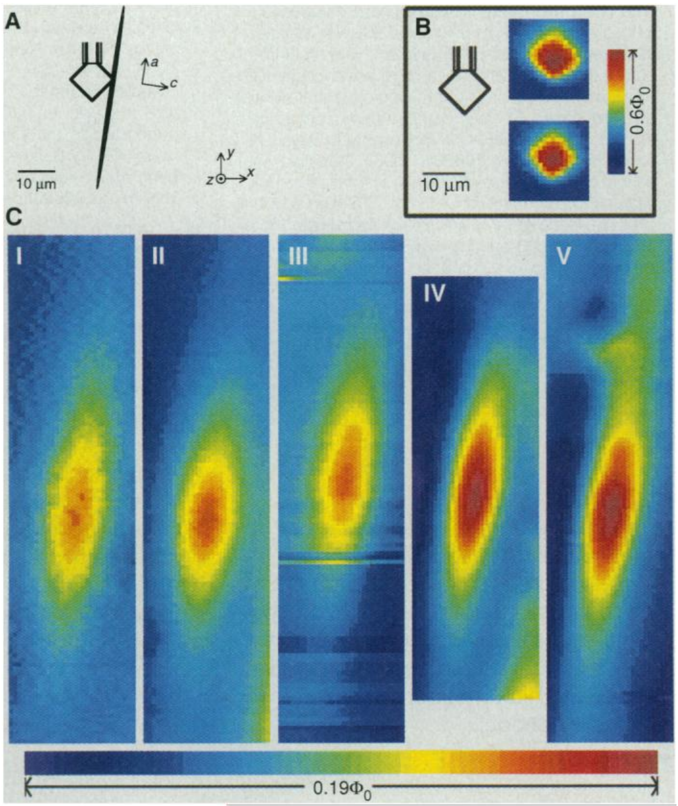

Fig. 1. (**A**) Sketch of an 8.2 μm by 8.2 μm pickup loop with shielded leads, together with a sketch of the magnetic fields of a highly anisotropic vortex. The flux through the pickup loop is given by the magnetic field B_z at a height $z_0 \approx$ 3 μm, integrated over the area of the pickup loop; *a* and *c* indicate the $Tl_2Ba_2CuO_{6+\delta}$ crystal axes. The extent of the vortex along the *a* axis is called the *c* axis or interlayer penetration depth, because it is determined by supercurrents flowing between the layers, parallel to *c*. (**B**) For comparison, images of two $YBa_2Cu_3O_{6.95}$ *ab*-plane vortices. Because these vortices are much smaller than 8.2 μm, their apparent shape is dominated by the shape of the pickup loop. (**C**) Images of $Tl_2Ba_2CuO_{6+\delta}$ *ac*-plane vortices. Vortices I, II, and III were observed in crystal 1; vortices IV and V were observed in crystal 2. The vortices are resolution-limited in the *c* direction but extend tens of micrometers along the *a* axis, indicating qualitatively that λ_c is a few tens of micrometers.

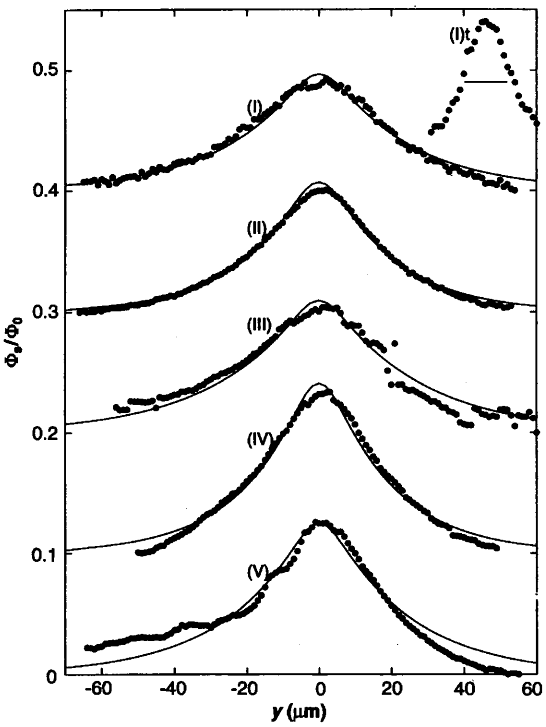

Fig. 2. Longitudinal cross sections along the *a* axis through the vortices from Fig. 1, plotted as the flux through the SQUID pickup loop, Φ_s (offset in $0.1\Phi_0$ increments) versus *y*. The data are fit to the functional form for the magnetic fields of an interlayer Josephson vortex with interlayer penetration depth λ_c, propagated to the height of the pickup loop above the surface, z_0, and integrated over the pickup loop. The fit parameters are: (I) $\lambda_c = 22^{+6}_{-4}$ μm, z_0 = 3.0 ± 0.6 μm; (II) λ_c = 18 ± 2 μm, z_0 = 3.4 ± 0.4 μm; (III) $\lambda_c = 25^{+10}_{-7}$ μm, z_0 = 2.0 ± 1.0 μm; (IV) λ_c = 18 ± 3 μm, z_0= 2.2 ± 0.6 μm; and (V) $\lambda_c = 22^{+11}_{-7}$ μm, z_0 = 1.9 ± 1.0 μm. A transverse cross section along *x* is also shown, with a scale bar indicating the extent of the pickup loop along *x*, 11.6 μm. The weighted average of the penetration depths is λ_c = 19 ± 2 μm.

The Tl-2201 crystals were grown under carefully controlled conditions (*20*). The crystals we chose for these experiments were platelet-shaped, with a basal plane area of ~1 mm^2 and a thickness along the c axis varying between 50 and 100 μm. The images were made in a magnetically shielded dewar with an unknown residual field of several milligauss. We observed many similar *ac*-plane vortices in different parts of the two crystals. Five vortices (Fig. 1C) were chosen for detailed analysis because of their relatively large spacing from neighboring vortices. The vortices extend a few tens of micrometers along the a axis, indicating qualitatively that λ_c is a few tens of micrometers. The full width at half-maximum (FWHM) along the a axis ranged from 35 to 46 μm (Fig. 2).

Neglecting the influence of the surface on the fields, and defining a and c as the directions parallel and perpendicular to the layers, respectively, the z-component of the magnetic field of an interlayer Josephson vortex is given by

$$b_z(x_c, y_a, z = 0) = \frac{\Phi_0}{2\pi\lambda_a\lambda_c} K_0(\tilde{R}) \qquad (3)$$

(*10*), where

$$\tilde{R} = [(s/2\lambda_a)^2 + (x_c/\lambda a)^2 + (y_a/\lambda c)^2]^{1/2} \qquad (4)$$

K_0 is a modified Bessel function of the second kind (of order 0), and x_c and y_a denote the distance along the c axis and a axis, respectively (*11*). In our images, the crystal axes are rotated by 9° from the scan axes (Fig. 1). For these experiments, $\lambda_a \ll (L, \lambda_c)$, so it is appropriate to integrate over x_c at the surface. After this integration, the FWHM along y_a is $\sqrt{2}\lambda_c$. For comparison with the experimental data, we propagated the fields to a height $z = z_0$ and integrated over the pickup loop (*12*). There are thus two nonlinear free parameters, z_0 and λ_c.

Fits to longitudinal cross sections (along the *a* axis) of vortices I to V are shown in Fig. 2. The error bars are determined using a criterion of doubling of the variance from the best-fit value. Taking the statistical average of the values of λ_c weighted by the inverse of the square of the error, we find $\lambda_c = 19 \pm 2$ μm. There are larger systematic errors, which we estimate to be <30%, associated with the uncertainties in the SQUID detector function (*19*) and with the uncertainty in the slope of the background.

We used a similar procedure to make 2D fits of the vortices as a consistency check. The fit shown in Fig. 3 has three additional linear free parameters, allowing a best-fit planar background. Because the transverse direction is resolution-limited, the approximations in the effective shape of the detector (*19*) produce more serious errors than for the 1D longitudinal fit. Although these fits slightly underestimate the longitudinal width, they agree with the results from the 1D fits to within about 20%.

The consistency of our images leads us to believe that we are seeing, within our resolution, the intrinsic vortex shape for *ac*-plane vortices in Tl-2201. However, this technique would not detect local materials defects that were homogeneously distributed over length scales of several micrometers or more. For example, if the crystals contained stacking faults or a superlattice structure, the coupling would vary along the *c* axis. The penetration depth measured from the size of the vortices would be dominated by the most weakly coupled layers. Our direct measurement of the interlayer penetration depth is consistent with the nonobservation of the Josephson plasma resonance down to a frequency of 100 cm^{-1} (*8*). If the Josephson plasma resonance is detected, a comparison of ω_p and λ_c might address the role of possible microscopic inhomogeneities. Superstructures and stacking faults could also be identified by transmission electron microscopy.

An empirical correlation between λ_c and the far-infrared *c*-axis conductivity for several cuprates has been reported by Basov *et al.* (*21*). If we substitute the Tl-2201 dc *c*-axis conductivity, $\sigma_{c,n} \approx 2$ (ohm·cm)$^{-1}$ (*8*), for the far-infrared *c*-axis conductivity, our measurement agrees with Basov's correlation. In this limited sense, the *c*-axis transport properties of Tl-2201 are not unconventional for a cuprate. However, the normal-state dc *c*-axis resistivity of Tl-2201 appears to be close to linear in temperature (*8*, *22*).

In several published models, the *c*-axis coupling is described as a tunneling process that is independent of the mechanism of superconductivity. First, for diffusive pair transfer (parallel momentum not conserved) and an isotropic gap, $J_0 = \pi\Delta / 2e\rho_\perp$ (*23*), where Δ is the energy gap and $\rho_\perp$ is the interplane normal-state resistivity per plane. If we use $\rho_c = 0.5$ ohm·cm (*8*) and estimate Δ as the Bardeen-Cooper-Schrieffer value $1.76k_BT_c$ (where k_B is Boltzmann's constant), the penetration depth should be ~6 μm. [Using $\rho_c = 0.01$ ohm·cm (*22*) leads to the prediction 1 μm.] Second, for diffusive pair transfer with an anisotropic gap, the penetration depth is increased by an amount that depends on the details of the gap and the transfer function (*24*), and should be >6 μm. Third, in the case of specular pair transfer (parallel momentum conserved), the critical current density would be $J_0 = \hbar/2\rho_\perp \tau e$, where τ is the scattering time. The experimentally measured value $(2\pi\tau c)^{-1} \approx 300$ cm^{-1} (*25*) then results in the estimate ~1 μm. Fourth, Fertig and Das Sarma's microscopic theory combines the Nambu-Gorkov formalism with a tight binding *c*-axis band and suggests that the effective-mass approximation substantially underestimates λ_c (*26*). Our single result may be consistent with these models, depending on the details of the scattering, the band structure, and the gap anisotropy.

In the ILT model, the penetration depth is quantitatively determined by the condensation energy. For Tl-2201, the prediction of the ILT model is $\lambda_{ILT} = 0.8$ to 2 μm (*3*, *4*, *8*, *10*). Leggett defined the parameter $\eta = (\lambda_{ILT}/2\lambda_c)^2$, the ratio of the *c*-axis kinetic energy in the superconducting ground state to the condensation energy (*4*). We find $\eta \approx 0.001$, indicating that the ILT mechanism can supply only about one-thousandth of the total condensation energy in Tl-2201. The direct measurement of $\lambda_c \approx 20$ μm in a high-T_c single-layer cuprate material represents a serious disagreement with the ILT model as a candidate mechanism for superconductivity, and can serve as a constraint on future theoretical work toward a complete understanding of the *c*-axis properties of the cuprates.

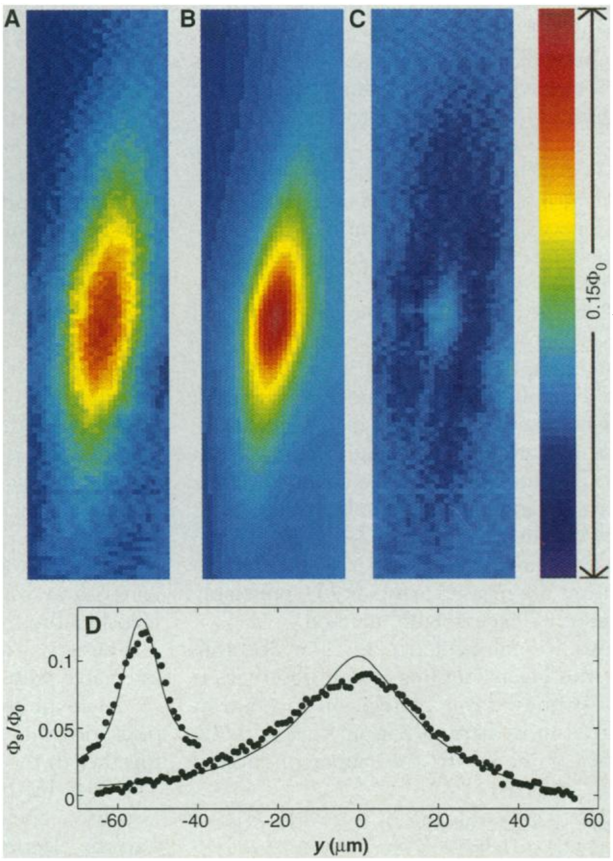

Fig. 3. (**A**) Vortex I. (**B**) A 2D fit to vortex I with $\lambda_c = 18$ μm and $z_0 = 3.6$ μm. Three additional linear free parameters allow an arbitrary planar background. (**C**) The difference between the data and the fit. (**D**) A cross section along the *a* axis and a cross section along the *x* axis, offset for clarity. Because of the systematic uncertainties in the background, the shape of the vortex, and the effective shape of the pickup loop, the value of λ_c obtained is 20% lower than the value obtained from the 1D fit in Fig. 2.

REFERENCES AND NOTES

1. Interlayer tunneling has been identified experimentally and is understood independently of the ILT model, which speculates that such tunneling is the mechanism of superconductivity.
2. J. Wheatley, T. Hsu, P. W. Anderson, *Nature* **333**, 121 (1968); P. W. Anderson, *Physica C* **185**, 11 (1991); *Phys. Rev. Lett.* **67**, 660 (1991); *Science* **256**, 1526 (1992); S. Chakravarty, A. Sudbø, P. W. Anderson, S. Strong, *ibid.* **261**, 331 (1993).
3. P. W. Anderson, *Science* **268**, 1154 (1995).
4. A. J. Leggett, *ibid.* **274**, 587 (1996).
5. S. Chakravarty, *Eur. Phys. J. B*, in press.
6. W. E. Lawrence and S. Doniach, in *Proceedings of*

the 12th International Conference on Low Temperature Physics, E. Kando, Ed. (Academic Press, Kyoto, Japan, 1971), p. 361.
7. L. N. Bulaevskii et al., Phys. Rev. B 55, 8482 (1997); K. Tamasaku, Y. Nakamura, S. Uchida, Phys. Rev. Lett. 69, 1455 (1992); O. K. C. Tsui, N. P. Ong, J. B. Peterson, ibid. 76, 819 (1996).
8. D. van der Marel, J. Schützmann, H. S. Somal, J. W. van der Eb, in Proceedings of the 10th Anniversary HTS Workshop on Physics, Materials, and Applications, B. Batlogg, C. W. Chu, W. K. Chu, D. U. Gubser, K. A. Müller, Eds. (World Scientific, Rivers Edge, NJ, 1996), p. 357; J. Schützmann et al., Phys. Rev. B 55, 11118 (1997).
9. C. Panagopoulos et al., Phys. Rev. Lett. 79, 2320 (1997).
10. P. W. Anderson, Science 279, 1196 (1998).
11. J. R. Clem and M. W. Coffey, Phys. Rev. B 42, 6209 (1990); ______, Z. Hao, ibid. 44, 2732 (1991); A. Gurevich, M. Benkraouda, J. R. Clem, ibid. 54, 13196 (1996).
12. J. R. Kirtley et al., Phys. Rev. Lett. 76, 1336 (1996).
13. J. R. Kirtley, K. A. Moler, J. M. Williams, J. A. Schlueter, unpublished data. BEDT-TTF is bis(ethylenedithio)-tetrathiafulvalene.
14. J. R. Kirtley et al., Appl. Phys. Lett. 66, 1138 (1995).
15. F. Zuo et al., Phys. Rev. B 47, 8327 (1993).
16. K. A. Moler, J. R. Kirtley, R. Liang, D. Bonn, W. N. Hardy, ibid. 55, 12753 (1997).
17. J. Pearl, J. Appl. Phys. 37, 4139 (1966).
18. A. M. Chang et al., Appl Phys. Lett. 61, 1974 (1992); Europhys. Lett. 20, 645 (1992).
19. Treating z_0 as a free parameter but neglecting the finite width of the wires of the pickup loop (0.8 μm), the field expelled by the shielded leads, and the angle between the loop and the surface (~20°), it is possible to describe the amplitude and shape of monopole (point-like) sources of magnetic flux to within 10%.
20. The Tl-2201 single crystals were grown from a flux in an alumina crucible with an alumina lid that was sealed to avoid loss of thallium oxide. Tl_2O_3, BaO_2, and CuO powders were mixed at the atomic ratio of Tl:Ba:Cu = 2.2:2:2 using excess Tl_2O_3 and CuO as the flux. The crucibles, containing ~50 g of charge, were loaded in a vertical tube furnace and heated rapidly to 925° to 950°C. This temperature was held for 30 min. The furnace was then cooled at about 5°C/hour to 875°C, and finally furnace-cooled to room temperature. The crystals were annealed for 3 days in flowing, gettered, high-purity argon at 400°C to remove any interstitial oxygen so as to obtain a high transition temperature. The ac faces were polished to optical flatness before imaging. The superconducting transition temperature was measured by ac susceptibility (ac applied field, 1 G) before polishing and magnetic imaging, and by dc field–cooled susceptibility (dc applied field, 1 G + Earth's field) after other measurements were complete. The transition temperatures and widths were T_c = 79 K, ΔT_c = 10 K (crystal 1, before), T_c = 74 K, ΔT_c = 11 K (crystal 1, after), T_c = 79 K, ΔT_c = 8 K (crystal 2, before), and T_c = 77 K, ΔT_c = 9 K (crystal 2, after).
21. D. N. Basov et al., Phys. Rev. B 50, 3511 (1994).
22. A. M. Hermann et al., in Proceedings of the Beijing International Conference: High Temperature Superconductivity (BHTSC '92), Z. Z. Gan, S. S. Xe, Z. X. Zhao, Eds. (World Scientific, Singapore, 1993), p. 445; H. M. Duan et al., Chin. J. Phys. 30, 415 (1992).
23. V. Ambegaokar and A. Baratoff, Phys. Rev. Lett. 10, 486 (1963); ibid. 11, 104 (1963).
24. M. J. Graf, D. Rainer, J. A. Sauls, Phys. Rev. B 47, 12089 (1993); A. G. Rojo and K. Levin, ibid. 48, 16861 (1993); P. J. Hirschfeld, S. M. Quinlan, D. J. Scalapino, ibid. 55, 12742 (1997).
25. A. V. Puchkov, Phys. Rev. Lett. 77, 3212 (1996).
26. H. A. Fertig and S. Das Sarma, Phys. Rev. B 44, 4480 (1991).
27. We thank P. W. Anderson, S. Chakravarty, S. Das Sarma, N. P. Ong, D. Scalapino, and D. van der Marel for useful discussions; D. Johnson for technical assistance in sample preparation; and M. Bhushan, M. Ketchen, and A. Ellis for assistance in the construction of the scanning SQUID microscope. Work at Argonne was supported by NSF grant DMR 91-20000 through the Science and Technology Center for Superconductivity, and by the U.S. Department of Energy under contract W-31-109-ENG-38. Work at Princeton was supported by NSF grant DMR 94-00362 through the Princeton Materials Institute, and by an R. H. Dicke Postdoctoral Fellowship.

3 November 1997; accepted 24 December 1997

c-Axis Electrodynamics as Evidence for the Interlayer Theory of High-Temperature Superconductivity

Philip W. Anderson

In the interlayer theory of high-temperature superconductivity, the interlayer pair tunneling energy (similar to the Josephson or Lawrence-Doniach energy) is the motivation for superconductivity. This connection requires two experimentally verifiable identities: the coherent normal-state conductance must be smaller than the "Josephson" coupling energy, and the Josephson coupling energy must be equal to the condensation energy of the superconductor. The first condition is well satisfied in the only case that is relevant, $(La,Sr)_2CuO_4$, but the second condition has been questioned. It is satisfied for all dopings in $(La,Sr)_2CuO_4$ and also in optimally doped $Hg(Ba)_2CuO_5$, which was measured recently, but seems to be strongly violated in measurements on single crystals of $Tl_2Ba_2CuO_6$.

The theory that ascribes the phenomenon of high–transition temperature (T_c) superconductivity in the cuprates primarily to interlayer coupling (*1*) correlates electromagnetic coupling along the *c* axis (that is, perpendicular to the CuO_2 planes) with the condensation energy of the superconductor. This correlation, which should be particularly sharp for "one-layer" materials, was proposed and roughly tested against data on $(La,Sr)_2CuO_4$ ("214") (*2*), and the equations were refined by van der Marel *et al.* (*3*) and Leggett (*4*). In these latter papers, the apparent failure of the relation in $Tl_2Ba_2CuO_6$ ("Tl 2201") was emphasized, and rather unequivocal measurements of the *c*-axis penetration depth λ_c (*5*) confirm this contradiction. However, there is quite good agreement in a growing number of other cases: 214 at several different doping levels (*6*) and $HgCa_2CuO_4$ (Hg "1201" cuprate) (*7*). It appears then, that the Tl salt is the "odd man out" or perhaps is not a true one-layer case; this compound exhibits wide swings in T_c with preparation treatment. Because both the Tl and Hg salts have relatively large *c*-axis spacings and comparable values of $T_c \approx 90$ K, the contradiction between the two is particularly striking, and it is important to confirm the measurements of (*7*), preferably by another experimental method.

Additional evidence for a major role for interlayer coupling is the observation of a strong bilayer correlation in neutron scattering in yttrium barium copper oxide (YBCO) both in the superconducting state (for optimal doping) (*8*) and in the spin-gap regime (*9*), which is not explicable in one-layer theories but is predicted by the interlayer theory (*10*). Thus, Tl 2201 stands out in providing contravening evidence against the theory of (*1*).

The interlayer theory is simple in principle. For the cuprates, electron motion in the *c* direction is incoherent in the normal state. This anisotropy is unlike most normal metals, which are Fermi liquids and exhibit coherent transport in all directions. The interlayer hypothesis is that electron pairing in the superconducting state makes this transport coherent, which is actually observed and is responsible for the Josephson-like or Lawrence-Doniach–like superconducting coupling between the layers. In conventional superconductors, the Lawrence-Doniach coupling replaces coherent transport in the normal state, so that the superconductor gains no relative energy, but in the cuprates, experimental observations exclude coherent transport in the normal state, so that the *c*-axis energy is available as a pairing mechanism. [In my theory (*1*), the mechanism blocking coherent transport is the non–Fermi liquid nature of the normal metal state.] Thus, superconductivity occurs in connection with a crossover from two-dimensional to three-dimensional transport; if one desires a "quantum critical point" to be associated with high T_c, that is its nature.

There are then two independent ways of measuring the energy that couples the planes together in the superconductor, each direct. The first method is, in analogy with the Josephson energy-current relation, to measure the electromagnetic response to vector

Joseph Henry Laboratories of Physics, Princeton University, Princeton, NJ 08544, USA.